Statistical Analysis of Ion Diffusion Region Characteristics Using Scalar Parameters

A.J. Rogers[1], C.J. Farrugia[1], R.B. Torbert[1]

[1]The University of New Hampshire, Department of Physics, Durham, NH

15 December 2021

Introduction

Reconnection regions have traditionally been identified using correlated magnetic field and plasma flow reversals in conjunction with Hall currents and reconnection electric fields (Rogers *et al.* 2019). While reasonably robust, these techniques depend on analyzing those qualities in a coordinate system well-aligned with structure of the reconnecting current sheet. Parameters independent of any coordinate system (scalar parameters) which can reliably indicate proximity to a reconnecting current sheet would greatly simplify the identification of reconnection events in *in situ* data.

Scalar parameters derived from direct field measurements and particle distribution functions such as the adiabatic expansion parameter and the $\sqrt{Q}$ parameter have been suggested as tools to identify or even define magnetic reconnection when applied to *in situ* electron measurements. The physics which suggest these parameters to describe electron diffusion and demagnetization are equally applicable to ions to describe the same effects. Additionally, a non-zero energy conversion rate ($\vec{J}\cdot\vec{E}$) is a common characteristic near a reconnecting X-line. Similarly, we expect strongly enhanced current density ($|\vec{J}|$) and a non-zero parallel electric field near the X-line due to charge separation and differential acceleration. Recent discussions have also revived the bulk ion velocity ($|\vec{V}_i|$) as an indicator of nearby reconnection. These are the parameters chosen for analysis

Methodology

Minimum and maximum values of each chosen parameter are calculated for each event window. Which of the maximum or minimum of each parameter is used in the analysis is dependant on the expected behavior near a reconnecting X-line. Principal Component Analysis (PCA) is then performed on all relevant extrema after being column-centered. The centered data is then projected into the space defined by the resulting principal component vectors (PCVs). Figures showing all 25 events in the space defined by the three most significant PCVs are shown to the right.

References

— Rogers, A.J, C.J. Farrugia, R.B. Torbert. (2019) "Numerical Algorithm for Detecting Ion Diffusion Regions in the Geomagnetic Tail with Applications to MMS Tail Season May 1– September 30, 2017". *JGR:Space Physics*. JGRA55058. doi:10.1029/2018JA026429.

— Scudder, J.D., R.D. Holdaway, R. Glassberg, S.L. Rodriguez. (2008) "Electron diffusion region and thermal demagnetization". *JGR. 113.* A10208.

— Swisdak, M. (2016) "Quantifying gyrotropy in magnetic reconnection". *GRL. 43.* 43-49.

— Shen, C., X. Li, M. Dunlop, Z. X. Liu, A. Balogh, D. N. Baker, M. Hapgood, and X. Wang. (2003). "Analyses on the geometrical structure of magnetic field in the current sheet based on cluster measurements". *JGR. 108. A5. 1168.* doi:10.1029/2002JA009612

Acknowledgements

Thanks are owed to: Matt Argall, Akhtar Ardakani, John Marci, Ivan Dors, Christine Schultz, Hiroshi Matsui, Dominic Payne, Chris Mouikis, Terry Forbes, Kevin Genestretti, Tim Rogers, Zach Dykstra, and Theresa Ward.

This work has been supported by NASA via contract 499878Q

Parameter	Expression
kappa:K	$K=\sqrt{\frac{r_{gyro}}{R_{curveature}}}$
Agyrotropy:$\sqrt{Q}$	$Q=\frac{4I_2}{(I_1-P_\parallel)(I_1+3P_\parallel)}$ $I_1\equiv \mathrm{Tr}(\bar{P}_i)$, $I_2\equiv$ sum of principal minors
Adiabatic Expansion parameter:Γ	$\Gamma_{\perp,i}=\frac{\lvert\vec{E'_\perp}+\vec{w_i}\times\vec{B}\rvert}{w_{\perp,i}B}:w_{\perp,i}\equiv\sqrt{\frac{2K_BT_{\perp,i}}{m_i}}$
Energy Conversion:	$\vec{J}\cdot\vec{E}$
Current Density:	$\lvert\vec{J}\rvert$
Parallel Electric Field:	$\vec{E}\cdot\hat{b}$
Bulk Ion Speed:	$\lvert\vec{V_i}\rvert$

Table: **1** List of the chosen scalar parameters, their expressions in terms of *in situ* measurements.

Parameter Statistics

	$min(\kappa)$	$max(\sqrt{(Q)})$	$max(\Gamma)$	$min(\vec{J}\cdot\vec{E})$	$max(\lvert\vec{J}\rvert)$	$min(\vec{E})$	$max(\lvert\vec{V_i}\rvert)$
$\overline{p}$	.2358	.2884	5.977	-1.471E-09	1.080E-07	-2.070E-02	552.2
σ_p	.5332	.0982	4.816	1.418E-09	7.411E-08	2.127E-02	172.9
p_{min}	.0362	.0398	.2579	-6.936E-09	1.617E-08	-9.200E-02	335.8
p_{max}	2.767	.4634	19.79	-4.859E-11	3.839E-07	-2.297E-03	899.6

Table: **2** Statistics of parameter extrema values across all 25 events

Eigenvectors

λ	$min(\kappa)$	$max(\sqrt{Q})$	$max(\Gamma)$	$min(\vec{J}\cdot\vec{E})$	$max(\lvert\vec{J}\rvert)$	$min(\vec{E}_\parallel)$	$max(\lvert\vec{V_i}\rvert)$
0.334	0.3200	-0.2031	0.0586	-0.9005	-0.0666	0.1932	-0.0170
0.240	-0.4393	0.2045	-0.1899	-0.2514	0.5820	-0.0214	-0.5717
0.047	-0.4832	-0.3378	0.6840	0.0367	0.0388	0.4251	0.0308
0.117	0.4341	-0.0805	-0.0967	0.2164	0.6731	0.4874	0.2415
0.106	-0.2445	0.5346	-0.3007	-0.0649	-0.3287	0.6555	0.1484
0.085	0.4706	0.2822	0.3787	0.1968	-0.1828	0.1979	-0.6665
0.072	0.0372	0.6564	0.4995	-0.1866	0.2469	-0.2740	0.3839

Table: **3** The eigenvectors resulting from PCA with weighted eigenvalues (λ). Note that eigenvectors are not in order ranked by eigenvalue.

Discussion

Once projected into the PCV space, the bulk of the previously identified IDRs are contained in a relatively compact region. Centered in that region are strong examples of IDRs and Electron Diffusion Regions (EDRs) such as event **E** which is the Torbert July 11, 2017 event as well as event **T** shown in figure **2**. Initial analysis shows that events with the strongest EDR approaches have relatively small components in the $\hat{e}_2$ and $\hat{e}_4$ directions and a strong negative $\hat{e}_1$ component.

The first eigenvector is dominated by $\vec{J}\cdot\vec{E}$ (see Table **3**). Events such as event **K** which are strongly positive in $\hat{e}_1$ would be expected to show little non-zero energy conversion. Outliers in the $\hat{e}_2$ are characterized by strong imbalances between κ, $|\vec{J}|$, and $|\vec{V_i}|$. For example, event **K** shows a strong enhancement in ion speed, with moderate current densities, but very little remarkable in κ. By contrast, event **Q** (not shown) has very small κ values with reasonably impressive current density peaks, but with ion speeds little greater than those found in event *K*.

Conclusion

Principal Component Analysis gives a means for rapidly categorizing IDRs. This can be applied in future to automated algorithms (*i.e.* machine learning) for event detection and initial classification for review.

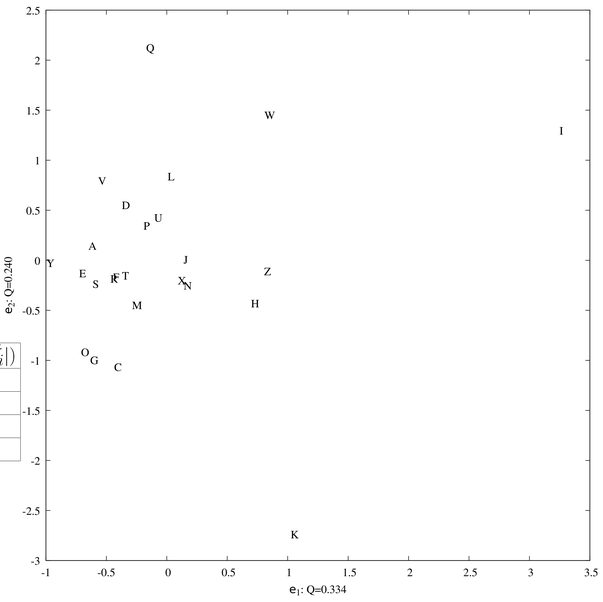

Figure: **1** All 25 analyzed events projected into the space formed by the first two PCVs

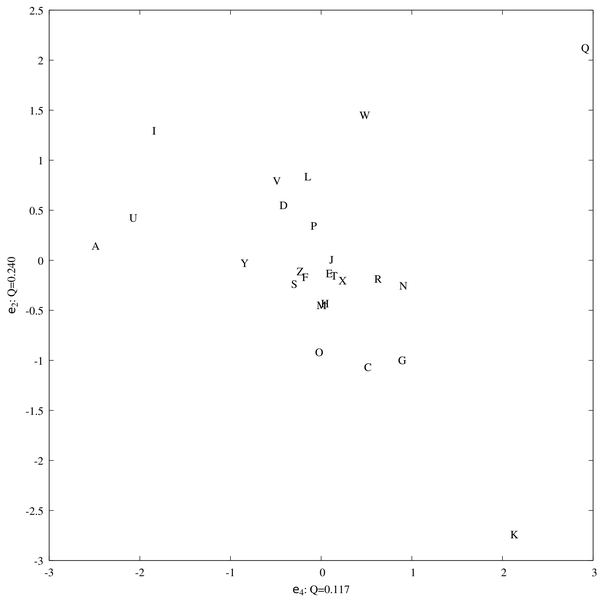

Figure: **3** All 25 analyzed events projected into the space formed by the 2nd and 4th PCVs

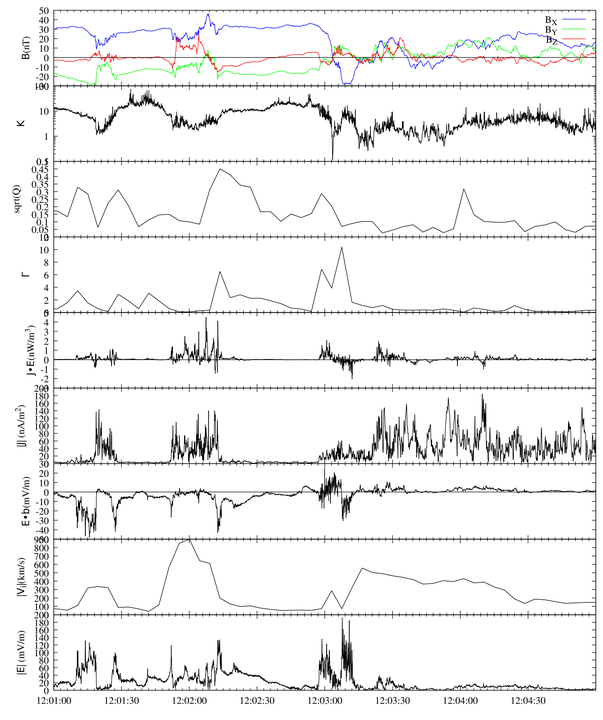

Figure: **2** Timeseries measurements of the selected scalar parameters (with $\vec{B}$ and $|\vec{E}|$ for context) for event **T**; a "good" IDR example

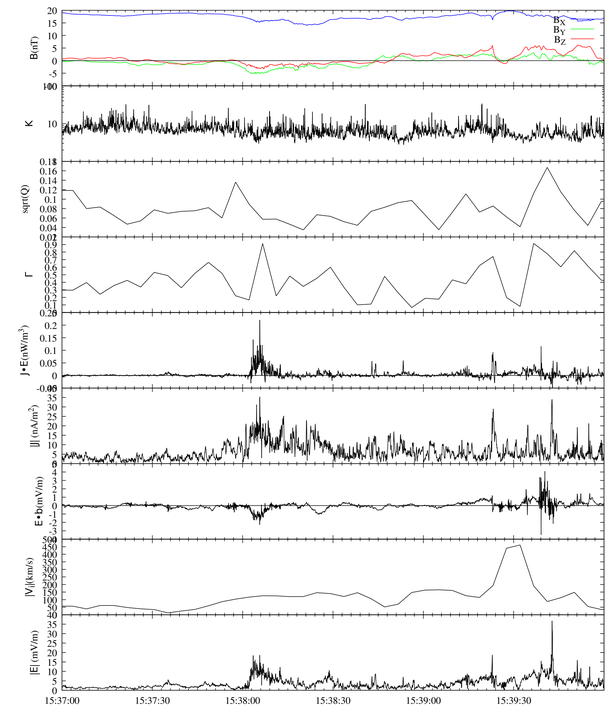

Figure: **4** Timeseries *ala* Fig.**2** of event **K**, a wide outlier identified using PCA